Received: 1 October 2018 | Revised: 11 January 2019 | Accepted: 9 February 2019

DOI: 10.1111/cbdd.13510

RESEARCH ARTICLE

WILEY

ER alpha selective chromone, isoxazolylchromones, induces ROS-mediated cell death without autophagy

Swati Kaushik[1,2] | **Rahul Sanawar**[1,3] | **Asha Lekshmi**[1] | **Leena Chandrasekhar**[1] | **Mydhily Nair**[1] | **Seema Bhatnagar**[2] | **Thankayyan Retnabai Santhoshkumar**[1]

[1]Cancer Research Program 1, Rajiv Gandhi Centre for Biotechnology, KINFRA Campus, Trivandrum, Kerala, India

[2]Novel Molecule Synthesis Laboratory, Amity Institute of Biotechnology, Amity University, Noida, Uttar Pradesh, India

[3]Manipal Academy of Higher Education (MAHE), Manipal, Karnataka, India

Correspondence
Thankayyan Retnabai Santhoshkumar, Cancer Research Program-1, Rajiv Gandhi Centre for Biotechnology, KINFRA Campus, Trivandrum, Kerala, India.
Email: trsanthosh@rgcb.res.in
and
Seema Bhatnagar, Amity Institute of Biotechnology, Amity University, Noida, Uttar Pradesh, India.
Email: sbhatnagar1@amity.edu

Funding information
DST | Science and Engineering Research Board (SERB), Grant/Award Number: PDF/2016/004001

Abstract

Chromones are recognized as privileged structures and useful templates for the design of novel compounds with promising pharmacological activity. Several reports implicate chromone scaffold as an antitumor agent. The present study highlights synthesis, docking, and potential activity of isoxazolylchromones, **3(a–f),** a new class of compounds as potential agents exhibiting ERα antagonism and ERβ agonism. Molecular docking studies determined the binding site of compounds **3(a–f)** in ERα and ERβ. All the analogues synthesized showed preferential cytotoxicity in ERα+ cell line (MCF-7) compared to ERα- cell line (MDA-MB-231). Among the analogues synthesized, analogue **3d** exhibited increased cytotoxicity. ERα silencing experiments confirmed the ERα selective nature of ligands. Transactivation assay on compound **3d** indicated the down-regulation of ERα luciferase reporter gene expression and induction of ERβ GFP in the treated cells. Cell cycle analysis revealed an increase in sub-G0/G1 population on treatment with analogue **3d** as compared to control. Similar to tamoxifen, **3d**-induced cell death is mediated through an increase in ROS as evidenced by change in roGFP ratio. Interestingly, the compound **3d** induced mitochondrial trans-membrane potential loss and caspase activation without indication of autophagy compared to tamoxifen that induced autophagy in the treated cells. Lack of significant autophagy and induction of ERβ signaling by the new compound place them as a better ERα antagonist.

KEYWORDS

autophagy, Caspase, cell cycle, estrogen receptor, isoxazolylchromones, ROS, SERM, transactivation

1 | INTRODUCTION

Estrogen receptor (ER) signaling is exceedingly complex and plays an essential role in both normal physiology and diverse pathological conditions including breast cancer. Although ER acts as ligand-activated transcription factors, the ER response is complex and cannot be explained by "classical concept" of receptor activation or deactivation upon ligand binding. A complex interplay of signaling cross talk comprising "genomic" and "non-genomic" pathways leads to transcriptional response. There is compelling evidence to indicate that elevated levels of the female sex hormone estrogen lead to a predisposition toward breast cancer (Henderson & Feigelson, 2000). As per estimates, nearly 70% of breast cancers express ER (Masood, 1992; Nilsson et al., 2001), and in these cases, estrogen is considered to promote tumor growth. Estrogen mediates its cellular signaling through two ER subtypes ER alpha (ERα) and ER beta (ERβ); both are members of the nuclear receptor (NR) superfamily (Heldring et al., 2007). Differential tissue distribution of ERα and ERβ adds to the

complexity of the problem. The alpha subtype has a more prominent role on the mammary gland and uterus whereas the beta subtype seems to have the more profound effect on the central nervous and immune system. In addition, ER beta signaling generally counteracts the ERα promoted cell hyperproliferation in tissues such as breast and uterus (Paterni, Granchi, Katzenellenbogen, & Minutolo, 2014). The estrogen receptor ligand-binding domain (LBD) has been the primary target for nuclear hormone receptor drug discovery. A comparison of LBD of ERα and ERβ indicates that they share a high degree of similarity in residues that line the binding cavity (Kuiper et al., 1997) while ER subtype selectivity is ultimately determined by structural differences in the LBDs of ERα and ERβ. Structural modeling by Minutolo and coworkers reported that residues in ERα and ERβ in contact with ligand differ at only positions: In helix 5, Leu384 of ERα corresponds to Met336 of ERβ and Met421 of ERα corresponds to Ile373 of ERβ in loop 6-7 (Minutolo, Macchia, Katzenellenbogen, & Katzenellenbogen, 2011). This difference confers variations in the total volume of ER isoforms LBD. The overall volume of the ligand-binding site is 490 $Å^3$ in ERα and 390 $Å^3$ in ERβ (Ottow & Weinmann, 2008). These differences can contribute to ligand selectivity on account of ring substitution, stereochemistry, and conformational orientation. Literature also indicates that the anchorage of a ligand into the receptor LBD is achieved by various interactions (H-bond, Van der Waals interaction) which most probably confer a broad spectrum of conformations leading to the recruitment of different sets of co-regulators (Laïos et al., 2007). Reports also suggest that ligands promote or prevent co-activator binding based on the shape of the estrogen or anti-estrogen receptor complex (Shiau et al., 1998).

Therapeutic agents that target the ER-positive cancers are referred to as selective estrogen receptor modulators (SERMs). Thus far, only five non-steroidal SERM and one steroidal anti-estrogen have been marketed (Maximov, Lee, & Jordan, 2013). For almost three decades, prototypical SERM, tamoxifen has been the drug of choice for the first-line therapy in both early and advanced ER-positive breast cancer (Peng, Sengupta, & Jordan, 2009). Unfortunately, long-term use of tamoxifen has been linked with undesirable side-effects and acquired resistance (Beato, Herrlich, & Schütz, 1995; Chang, Kim, Malla, & Kim, 2011; Farhat, Lavigne, & Ramwell, 1996; Turner, Riggs, & Spelsberg, 1994). Even though diverse mechanisms of hormone resistance are reported; induction of various survival signaling including autophagy is a major concern. It has been reported that tamoxifen and most of the currently used SERM are capable of eliciting protective autophagy in the target cells (Hongyi et al., 2017; Sommer & Fuqua, 2001).

In this regard, efforts to discover and develop new and more specific subtype-selective ligands, whether they are agonist or antagonist, have re-energized search for new chemical entities that may tackle this challenge. A literature search on bioactive natural metabolites indicates that chromone scaffold possess a wide spectrum of biological activity (Pick et al., 2011). Most prominently the chromone scaffold has been explored for anticancer properties (Middleton, Kandaswami, & Theoharides, 2000; Momoi et al., 2005). In the current study, we have aimed to identify ER subtype-selective ligands from several new isoxazolylchromones **3(a–f)**. Docking studies, dose–response analysis, gene silencing experiments, transactivation assay, GFP-labeled ERβ assay, cell cycle analysis, apoptotic studies, ROS induction, and autophagic analysis have confirmed the new ligands as a potential ERα selective antagonist. The studies also emphasize that the lead molecule elicits less cell survival signaling and increased ERβ agonist activity.

2 | METHODS AND MATERIALS

2.1 | Cell culture and gene silencing experiments

MCF-7 cells were grown in monolayer culture in RPMI-1640 (Sigma Chemicals Co., USA) supplemented with 10% heat-inactivated fetal bovine serum (FBS) and antibiotics in a humidified atmosphere of 5% CO_2 at 37°C. For silencing experiment, cells were seeded in the 6-well plates at desired densities. (a) Gene silencing using ERα siRNA on MCF-7 Cells: MCF-7 cells were transfected with ERα siRNA (Santa Cruz, #SC 29305) using oligofectamine (Invitrogen, #12252-011) according to manufacturer's protocol. (b) Drug Addition: For drug treatment, after overnight culture of cells in 6-well plates, the medium was replaced with fresh DMEM containing 5% FBS and the compounds to be tested. For imaging, 5% FBS containing phenol red-free DMEM was used. Concentrated stocks of compound **3d** and 4HT were prepared in DMSO and stored at −80°C. (c) Live Cell Staining–Hoechst 33342 staining: Hoechst 33342 is a popular cell-permeant nuclear stain that emits blue fluorescence when bound to double-strand DNA at A-T rich regions. Following treatment with compound **3d** at different concentrations and known drug 4HT, ERα gene silenced and non-silenced MCF-7 cells were stained with 2 μg/ml Hoechst 33342 (Molecular Probes #H1399) in phenol red-free DMEM containing 5% FBS by incubating at 37°C for 10 min. After washing twice with PBS, Hoechst 33342 fluorescence intensity was imaged for detecting pyknotic nuclei using DAPI filter set under the fluorescent microscope (Nikon TiE). Images were analyzed using NIS elements software. (d) SDS–PAGE and Western blotting: The MCF-7 cells treated with (ERα siRNA) or with vector control siRNA were washed with PBS and lysed using phosphorolysis buffer supplemented with protease inhibitors. After lysis, the suspension was centrifuged at 12,000 rpm for 20 minutes and the supernatant containing the whole cell

proteins was immediately estimated for protein, denatured, and resolved by SDS–PAGE. The protein concentration for each sample was estimated using Bradford's method. Protein samples were denatured in sample buffer containing β-mercaptoethanol and SDS at 100°C for 8 min and resolved in a 10% acrylamide gel. Equal amount of protein from the whole cell lysates of MCF-7 cells transfected with control siRNA and ERα siRNA was loaded and electrophoretically run along with prestained protein marker at a constant voltage of 80 V through the stacking gel and at 100 V through the separating gel. The resolved bands in the SDS–PAGE were electroblotted onto nitrocellulose membrane (Hybond-C pure, Amersham) using Bio-Rad Mini-PROTEAN III wet blot apparatus at 70 V for 2 hr in ice. After the transfer, the blots were washed with TBST buffer for 10 mins. The blotted membrane was blocked with 10% non-fat milk in Tris-buffered saline (TBS) containing 0.2% Tween-20 for 1 hr at room temperature to avoid the non-specific binding. Specific proteins were detected by incubating overnight with appropriate primary antibody in TBST buffer containing 5% BSA at 4°C followed by incubation with secondary antibody coupled with alkaline phosphatase or horse-radish peroxidase conjugates. (The primary antibodies were mouse anti-ERα (#SC-8002), mouse anti-β-actin (#A1978) purchased from Santa Cruz, USA and Sigma Chemicals Co., USA; used at 1:350 and 1:1,000 dilution, respectively. The secondary antibodies used were horse-radish peroxidase (HRP) labeled anti-mouse secondary antibodies (Sigma Chemicals Co., USA) at 1:4,000 dilution). The bands were developed with 3,3′-diaminobenzidine (DAB/H_2O_2) in 50 mM Tris, pH 7.6 or using enhanced chemiluminescence as per the manufacturer's protocol.

2.2 | Transfection and Luciferase reporter gene assay

MCF-7 cells after attaining 60%–70% confluency, 10% FBS containing DMEM media supplemented with antibiotic was removed and replaced with 5% charcoal-treated FBS containing media to reduce the contaminating steroids from the serum. After 4 hr, cells were transfected with pGL3-(ERE)-Luc plasmid (400 ng) using Lipofectamine® LTX and Plus™ reagent kit (Invitrogen.Cat.15338100) according to manufacturer's protocol. To evaluate the efficiency, 100 ng of SV40-Renilla luciferase (pRL-SV40) vector (Promega Madison, USA) was used as internal control for normalization. The plate was then incubated for another 20 hr in the humidified 5% CO_2 incubator. After 20 hr of transfection, cells were subjected to media containing either **3d** or 4HT separately and the plate was then kept back for another 24 hr. After 24 hr, luciferase assay was performed (according to the protocol of kit provided by Promega Madison, USA). The luciferase readings for each protein lysate were normalized to the Renilla luciferase readings. Estradiol was used at the concentration of 0.0005 μg/ml, and 4HT was used at a final concentration of 5.63 μg/ml.

2.3 | ERβ-GFP reporter assay

ERβ-EGFP expressing MCF-7 cells were generated using FuGENE® HD Transfection reagent according to manufacturer's protocol (Promega, Madison, WI 53711 USA); pEGFP-C1-ER beta plasmid was purchased from Addgene (plasmid #28237) (Addgene, Cambridge, MA 02139, USA). Homogeneously expressing single-cell colonies were selected using 800 μg/ml G418 antibiotic selection (Invitrogen, Carlsbad, CA) followed by FACS sorting. For live cell imaging, the ERβ-EGFP cells were seeded on a chambered cover glass (Lab-Tek, Nunc, Rochester, NY, USA) and grown in DMEM containing 10% FBS. Once the cells reached a confluency of 80%, the spent media was replaced with phenol red-free DMEM supplemented with 5% charcoal-treated FBS to reduce the contaminating steroids from the serum. After 4 hr, cells were treated with compound **3d** (32 μg/ml), estradiol (0.0005 μg/ml), and 4HT (5.63 μg/ml). Imaging was carried out using a Leica SP8WLL laser scanning confocal microscope. The images were captured using the 20X objective, and the emission was collected at 500-550 nm after exciting at 488 nm.

2.4 | ROS analysis using roGFP cells

Breast cancer cells were transfected with plasmid encoding for redox-sensitive GFP, roGFP2 using FuGENE ® HD transfection reagent according to manufacturer's protocol (Promega, Madison, WI, USA). The stable cells expressing roGFP were developed after G418 selection for 2 months. For the analysis of roGFP by flow cytometry, cells were seeded on 24-well plates and treated with 4HT (4HT-1 = 5.63 μg/ml; 4HT-2 = 11.26 μg/ml) and **3d** (**3d**-1 = 32 μg/ml and **3d**-2 = 64 μg/ml). The cells were trypsinized and analyzed using FACS AriaIII equipped with 405 and 488 nm laser lines. The emission was collected using 530/30 filter from the two laser paths in ratio mode. The cell population with increased 405/488 ratio from untreated cells were gated to calculate the percentage of cells with an increase in ROS. For microscopic imaging of roGFP, cells were grown on glass bottom plates and treated as above. The emission was collected at 515 ± 15 nm after exciting using 405 and 488 filter sets in ratio mode using NIS element software utilizing fully motorized fluorescent microscope (Nikon TiE).

2.5 | Autophagy analysis using MCF-7 LC3 GFP cells

MCF-7 cells were transfected with plasmid encoding LC3 GFP using FuGENE® HD transfection reagent according to manufacturer's protocol (Promega, Madison, WI 53711 USA). The

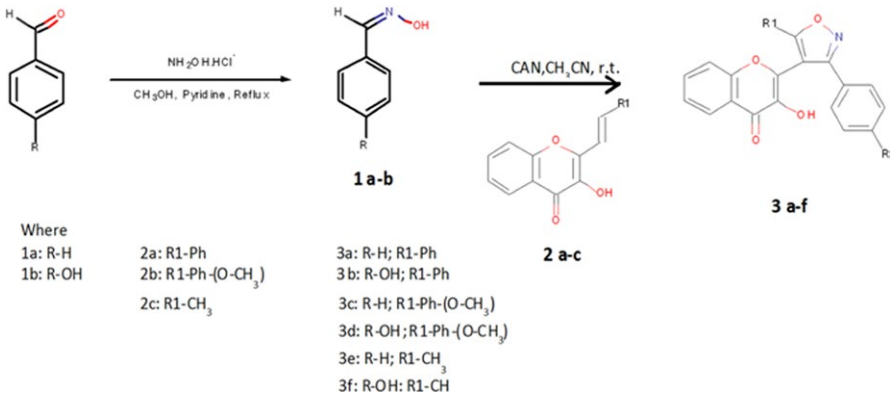

FIGURE 1 Illustrates scheme for the synthesis of isoxazolylchromones **3(a–f)**

cells were stained with TMRM and then were exposed to **3d** at its IC_{50} (32 μg/ml) value and 4HT at 2.81 μg/ml for 24 hr. The autophagy-specific aggregation of LC3 GFP was analyzed using GFP and PE filter sets under the fluorescent microscope, and the images were analyzed using NIS element software. Cells with more than 15 GFP punctae were scored as autophagic.

2.6 | Cell cycle analysis by propidium iodide stain

MCF-7 cells seeded in 60-mm dishes (2×10^4 cells/ml) overnight were treated with three concentrations of 4HT (5 μg/ml, 10 μg/ml, and 20 μg/ml) and analogue **3d** (15, 30, 60 μg/ml) for 48 hr. Cells were trypsinized, washed twice with ice-cold PBS, and fixed with ice-cold 70% ethanol. The cell pellet was stained with propidium iodide for cell cycle analysis after RNAase treatment and analyzed using BD FACS Aria III. The single-cell population identified were gated for sub-G0 apoptotic cells using FACS Diva 7.0 software and analyzed.

2.7 | Caspase activation analysis

(a) Image acquisition: The breast cancer cells (MCF-7 SCAT3 NLS) expressing a FRET-based caspase sensor were described earlier (Joseph, Seervi, Sobhan, & Santhoshkumar, 2011). For the detection of caspase activation, the stable cells were seeded in 96-well glass bottom plates at the desired density. After overnight culture, the medium was removed and replenished with phenol red-free DMEM containing 5% FBS containing the known drug 4HT (5.63 μg/ml) as a positive control and compound **3d** to be tested at its IC_{50} value. Plates were imaged under BD Pathway™ 435 Bioimager (Becton Dickinson Biosciences, USA). The excitation/emission filter for ECFP and EYFP FRET filter was used as described earlier (Joseph et al., 2011). Image for each well was acquired in the respective channels using a dry 20X objective with NA 0.7. Images were captured as 2×2 montage. (b) Postacquisition segmentation and analysis: Postacquisition image analysis was done using BDAttoVision™ (version 1.6/435, Becton Dickinson Biosciences, USA) by applying simple polygon segmentation, for nuclear regions identification using threshold level with FRET ratio loss (increased DEVDase activity) corresponding to increased ECFP/EYFP ratio signal. The results of FRET loss corresponding to increased ECFP/EYFP ratio were used to identify cells with caspase activation. Based on this, the percentage of cells with caspase activation was scored for each treatment as compared with control.

2.8 | Molecular docking protocol

Protein preparation: The ER PDB (http://www.pdb.org) IDs retrieved were 3ERT (Shiau et al., 1998), 2QTU (Richardson et al., 2007), and 2FSZ (Wang et al., 2006), respectively. The crystal structure was prepared with the help of the protein preparation wizard from the workflow option of the Maestro 9.3 Schrodinger suite. The water molecules were deleted, hydrogens were added, bond orders were assigned, and N-acetyl and N-methyl amide capping groups were added to the N-terminus and C-terminus, respectively. Finally, a restrained minimization of the receptor model was performed setting the default constraint of RMSD of 0.30 Å and OPLS 2005 force field. The first minimization was performed constraining the heavy atoms in order to allow free rotation of the hydrogen. Subsequently, minimizations were performed by decreasing the constraints on the heavy atoms. *Receptor grid preparation*: The 3D structure of ER was prepared using all three PDB entries and was used to generate Glide scoring grid for the successive docking calculations. The receptor grid box of size (10-10-10 $Å^3$) was generated with the centroid of the active site residues. Default parameters were used, and no constraints were included during grid generation. *Ligand preparation*: The 3D structures of the ligands were generated using Maestro, and the geometry of ligands was optimized by molecular mechanics using IMPACT (Banks et al., 2005) in a dynamic environment using standard TIP4P water model.

TABLE 1 Illustrates the docking score and glide energy of **3(a–f)** against ERα and ERβ

		Ligand-binding site of 4HT in ERα		Ligand-binding site of benzo-pyran ligands in ERβ		First binding site of 4HT in ERβ		Second binding site of 4HT in ERβ	
		3ERT		2QTU		2FSZ-101		2FSZ-103	
Compound name	**Compound structure**	**Docking score**	**Glide energy (Kcal/mol)**	**Docking score**	**Glide energy (Kcal/mol)**	**Docking score**	**Glide energy (Kcal/mol)**	**Docking score**	**Glide energy (Kcal/mol)**
3a	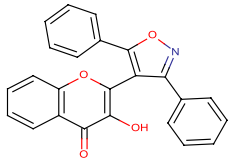	−7.68	−43.76	−6.94	−16.99	−6.89	−25.7	−2.36	−31.02
3b	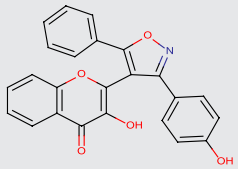	−8.24	−47.18	−7.39	−19.57	−7.81	−36.87	−3.01	−28.16
3c	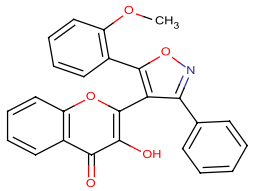	−7.33	−46.03	−5.02	−15.82	−7.02	−36.63	−2.07	−28.49
3d	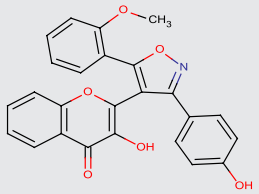	−8.71	−43.26	−6.82	−16.57	−7.84	−33.73	−2.73	−32.51
3e	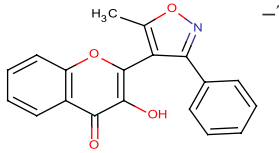	−7.42	−42.35	−8.68	−41.43	−6.08	−31.21	−3.38	−29.07
3f	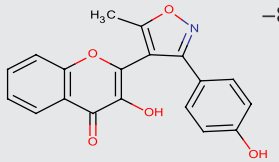	−8.71	−45.09	−8.59	−44.51	−6.74	−33.73	−2.98	−26.19

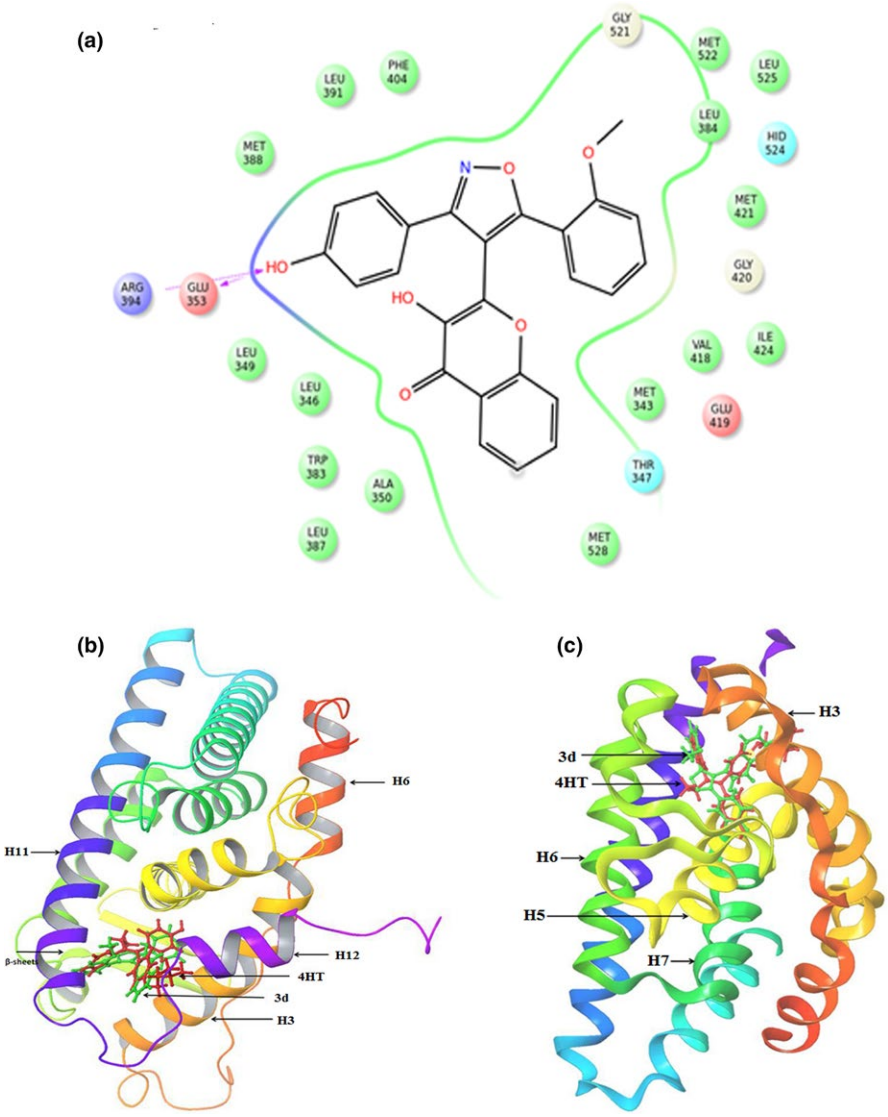

FIGURE 2 (a) Illustrates the ligand interaction map of **3d** with residues in 3ERT and its interactions with key residues Arg394 and Glu353. Also shown here is the ribbon model representation of the three-dimensional structure of ERα (b) and ERβ (c) docked with compound **3d** shown in green color, and superimposition with 4HT is depicted in red color

The conformational models of the ligands were generated using ligand preparation wizard (LigPrep.) Software tools LigPrep2.2 and Epik1.6 were used to compute the probable protonation states at pH 7.0 ± 3.0, all tautomers and up to 32 stereoisomers for compounds. The energy minimization was done using Optimized Potentials for Liquid Simulations 2005 (OPLS 2005) force field. Energy minimization was done using Polak–Ribiere conjugate gradient and Truncated Newton conjugate gradient algorithms. The convergence threshold of rms gradient of 0.01 was used. Conformational models of the ligands were generated using LigPrep. The lowest energy conformations of the ligands were used for docking with the receptor model. *Docking and scoring protocols*: The docking studies were carried out between all the model of ER and the different conformations of the ligands. All docking calculations were carried out using extra precision (XP) in built-in Glide (Grid-based Ligand Docking with Energetics). For the flexible docking mode, a set of conformers for each input ligand were generated by Glide after which an exhaustive search for possible positions and orientations of ligand over the active site were performed. The ligand poses generated by Glide are then passed through a series of hierarchical filters that evaluate the interaction of the ligand with the receptor. The OPLS-2005 force field was used for this purpose. A small number of surviving docking solutions can then be subjected to a Monte Carlo procedure to try and minimize the energy score. The final energy evaluation was done with Glide Score, and a single best pose was generated as the output for a particular ligand. These minimized poses are rescored using *Glide Score (G-Score)* scoring function. Model energy score (*E model*) was selected as the final scoring function to select the best-docked structure for each ligand. E model combines Glide Score with the non-bonded interaction energy between the ligand and the protein, the energy grid score, and (for flexible docking) the ligand strain energy. The different conformations of the known ligands were docked, and 1,000 poses per compound were

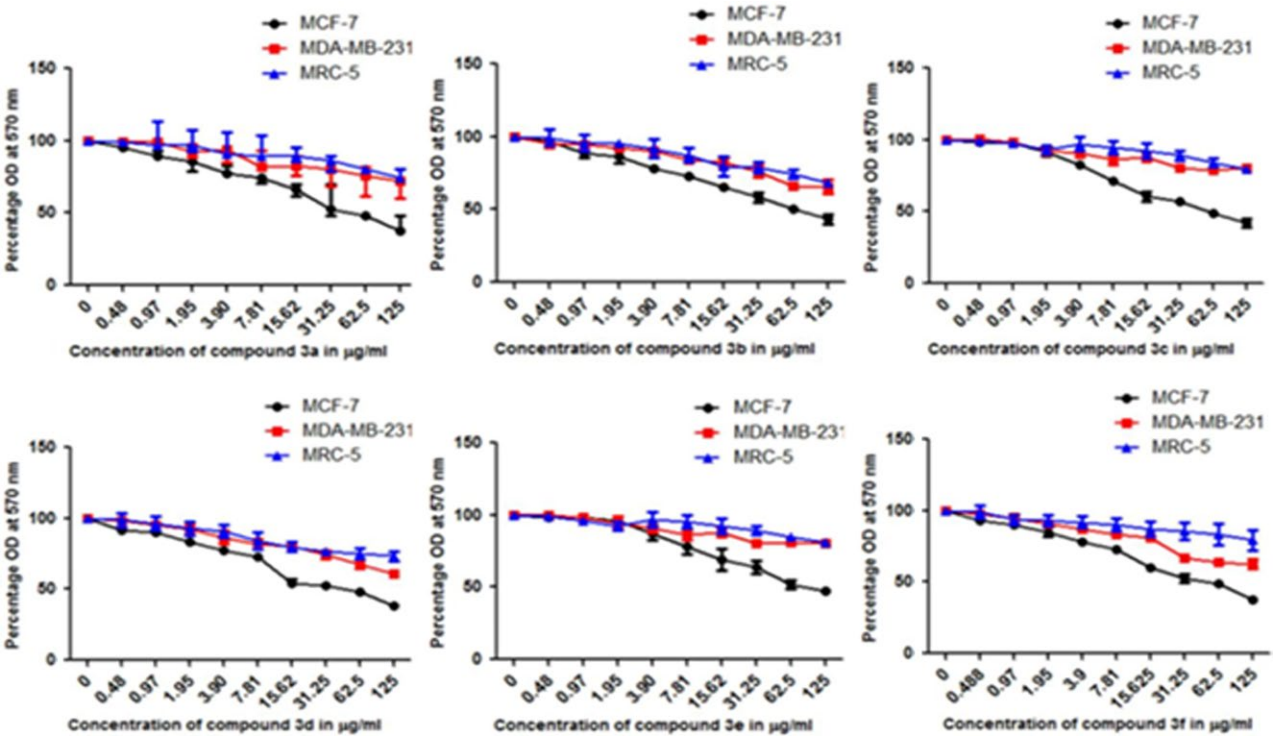

FIGURE 3 Dose-dependent studies of isoxazolylchromones **3(a–f)** plotted against % change in optical density at 570 nm in MCF-7, MDA-MB-231, and MRC-5 cell lines via MTT assay. The data are means and SEM from three samples of each group. Two-way ANOVA followed by Bonferroni post-test where *p*-value <0.05 is significant for compounds

obtained. The analysis of the poses, complexes, and the binding affinities between the receptor and ligands were analyzed using Schrodinger's software suite.

2.9 | Statistical analysis

The experimental results were expressed as mean ± standard error of the mean of four replicates. Where applicable, the data were subjected to one-way and two-way analysis of variance (ANOVA) followed by Bonferroni post-test using GraphPad Prism (version 5.1). *p*-value of ≤0.05 was regarded as significant.

3 | EXPERIMENTAL

3.1 | General procedure for the synthesis of Benzaldoxime (1a–b)

Synthesis of benzaldoxime was performed according to the reported procedure (Das, Mahender, Holla, & Banerjee, 2005).

3.2 | General procedure for the synthesis of 3-hydroxy-2-[3′, 5′-substituted isoxazole-4′1-yl]-4-chromone 2(a–f)

A benzaldoxime (**1a-b**, 1 mmol) and a 2-vinylchromone (**2a-c**, 1.2 mmol) were taken in acetonitrile (10 ml). CAN (2.2 mmol) was added and the mixture was stirred at room temperature. After 5 hr of reaction, TLC was monitored and the product was extracted with EtOAc. The extract was washed with water (3 × 10 ml), dried (Na_2SO_4), and concentrated. The crude was subjected to column chromatography over SiO_2 (60–120 mesh) using hexane: ethyl acetate 20% as eluent to give the desired isoxazolyl derivatives **3(a–f).**The spectral and analytical data of isoxazolylchromones are given below.

3a. 3-hydroxy-2-[3′,5′-diphenylisoxazol-4′-yl]-4-chromone obtained as semisolid from 2-vinylchromone (**2a**) and benzaldoxime (**1a**), IR (KBR, cm^{-1}): 3444 (OH), 1748 (C=O),1687 (C=N); ^{1}H NMR (500 MHz, DMSO, rt): δ 6.91-8.08 (14H,ArH), 9.79 (s,1H,OH); ESI-MS m/z: 382.38 ($M^+ + 1$).

3b. 3-hydroxy-2-[3′-(4-hydroxyphenyl)-5′-phenylisoxazol-4′-yl]-4-chromone obtained as semisolid from 2-vinylchromone (**2a**) and benzaldoxime (**1b**), IR (KBR, cm^{-1}): 3460(OH), 1795 (C=O), 1670 (C=N); ^{1}H NMR (500 MHz, DMSO, rt): δ 7.11-8.74 (13H,ArH), 9.97 (s,2H,OH); ESI-MS m/z: 420.369 (M^+ + Na).

3c. 3-hydroxy-2-[5′-(2-methoxyphenyl)-3′-phenylisoxazol-4′-yl]-4-chromone obtained as semisolid from 2-vinylchromone (**2b**) and benzaldoxime (**1a**), IR (KBR, cm^{-1}): 3250 (OH),1758 (C=O), 1685 (C=N); ^{1}H NMR (500 MHz, DMSO, rt): δ 4.04-4.22 (m,3H,O CH_3), 6.60-8.89 (13H, ArH), 9.98 (s,1H,OH); ESI-MS m/z: 411.40 $(M)^+$.

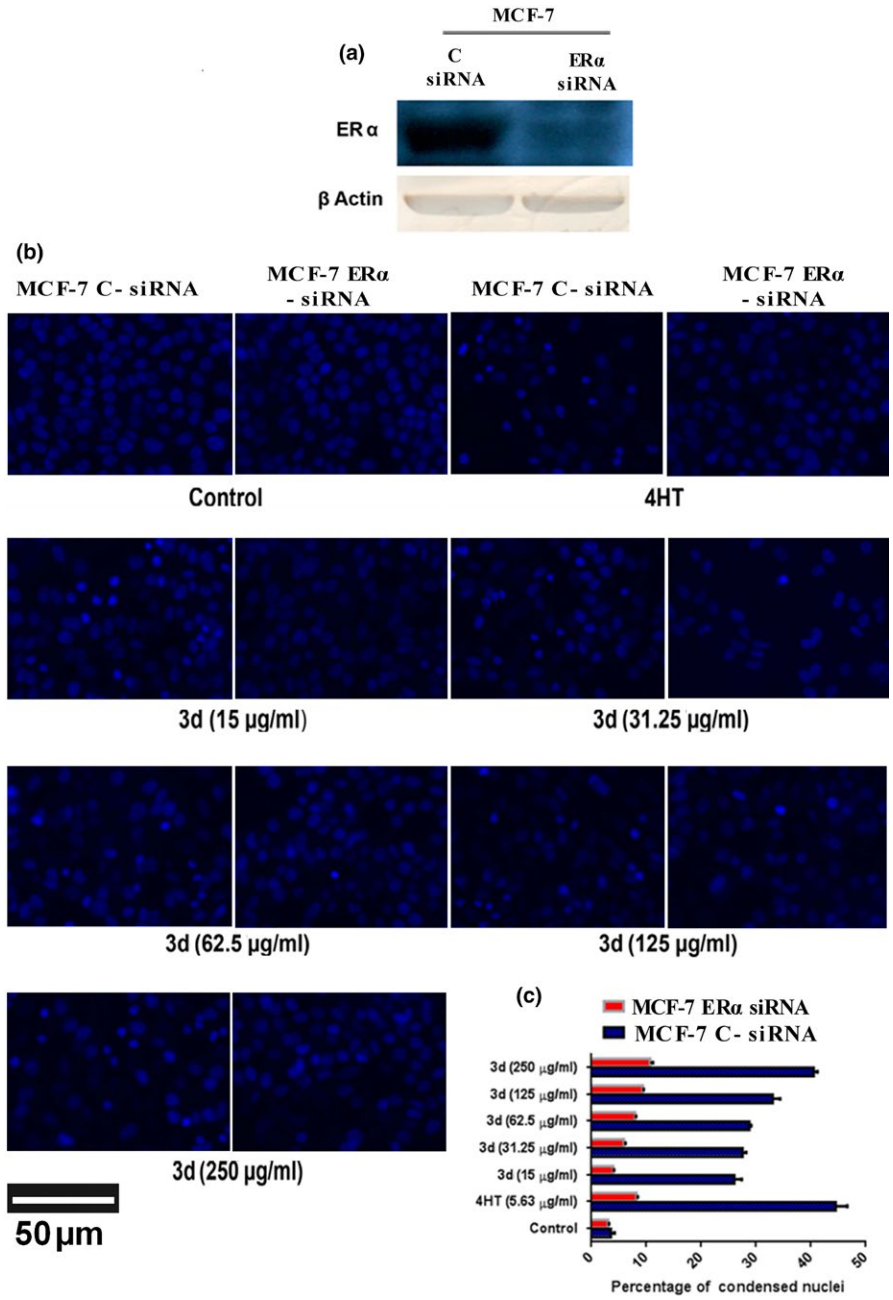

FIGURE 4 (a) Gene silencing experiment. Expression of ERα protein assessed by Western blot after transfecting with ERα siRNA. The difference in the expression of ERα in silenced as compared to parent MCF-7 cells is shown. (b) Effect of 4HT and **3d** on induction of apoptosis in parental (cells transfected with control siRNA) and silenced cells (cells transfected with ERα siRNA). Parental and ERα silenced MCF-7 cells were assessed for nuclear condensation following 48 hr treatment with 4HT (10 µM) and **3d** (15, 31.25, 62.5, 125, 250 µg/ml) by Hoechst staining. (c) Data are expressed as Mean±SD of nuclear condensation expressed as a percentage ($n = 3$). Two-way ANOVA followed by Bonferroni post-test where p-value <0.05 is significant. Scale bar = 50 µm

3d. 3-hydroxy-2-[3′-(4-hydroxyphenyl)-5′-(2-methoxyphenyl)-isoxazol-4′-yl]-4-chromone obtained as semisolid from 2-vinylchromone (**2b**) and benzaldoxime (**1b**), IR (KBR, cm^{-1}): 3420 (OH),1730 (C=O),1650 (C=N); ^{1}H NMR (500 MHz, DMSO, rt): δ 3.80-3.93(m,3H,O CH_3), 6.90-7.84 (12H, ArH), 8.48 (s,2H,OH); ^{13}C NMR (300 MHz, DMSO, rt):δ 64.82 (CH_3), 112.64–143.55 (12CH), 112.64-143.55 (6C), 156.27–166.42 (5C), 182.13 (C=O); ESI-MS *m/z*: 428.41($M^+ + 1$).

3e. 3-hydroxy-2-[5′-methyl-3′-phenylisoxazol-4′-yl]-4-chromone obtained as semisolid from 2-vinylchromone (**2c**) and benzaldoxime (**1a**), IR (KBR, cm^{-1}): 3,206 (OH), 1,769 (C=O), 1,632 (C=N); ^{1}H NMR (500 MHz, DMSO, rt):δ 2.49 (s, 3H, CH3), 6.66–7.88 (9H, ArH), 8.47 (s, 1H, OH); ESI-MS *m/z*: 319.31 $(M)^+$.

3f. 3-hydroxy-2-[3′-(4-hydroxyphenyl)-5′-methylisoxazol-4′-yl]-4-chromone obtained as semisolid from 2-vinylchromone (**2c**) and benzaldoxime (**1b**), IR (KBR, cm^{-1}): 3,350 (OH), 1,752 (C=O), 1691(C=N); ^{1}H NMR (500 MHz, DMSO, rt):δ 3.30–4.09 (m, 3H, CH3), 6.87–8.46 (8H, ArH), 10.90 (s, 2H, OH); ESI-MS *m/z*: 374.27 ($M^+ + K$).

4 | RESULTS

4.1 | Synthesis of isoxazolylchromones 3(a-f)

A small library of isoxazolylchromones was synthesized using 1, 3-dipolar cycloaddition reactions by reaction between nitrile oxides and 2-vinylchromones as dipolarophiles.

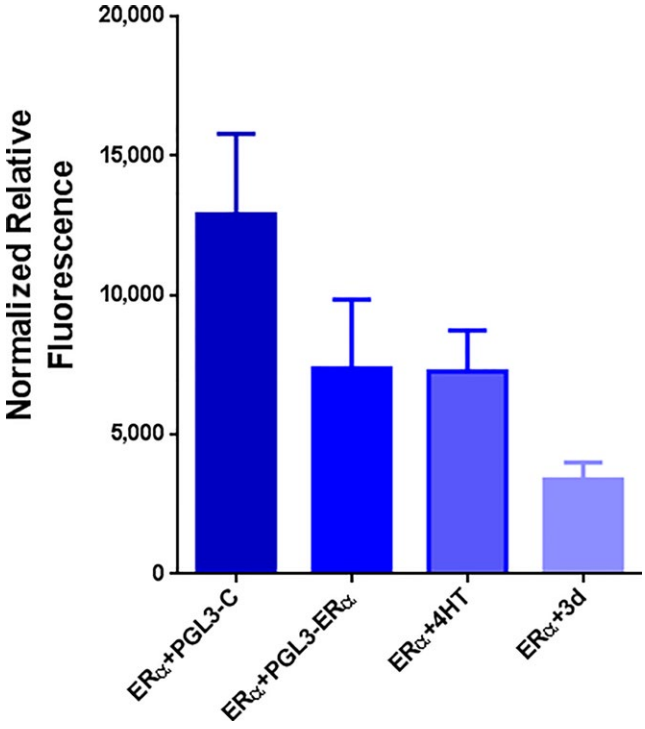

FIGURE 5 Transactivation analysis to show the effect of **3d** and 4HT in regulating ERα in MCF-7 cells. The data are mean ± SEM of three independent experiments performed in triplicates—one-way ANOVA where p-value <0.05 is significant

Our initial attempt to generate nitrile oxides from aldoximes using NBS in the presence of triethylamine in aprotic solvents at 0ºC and further trapping them by dipolarophile-2-vinylchromones resulted in a mixture of products which were difficult to isolate using column chromatography. As an alternative strategy, ceric ammonium nitrate (CAN) was used for generation of nitrile oxides (Das et al., 2005) from benzaldoximes (**1a-b**). The resulting nitrile oxides were trapped by 2-vinylchromones (**2a-c**). This method successfully resulted in various derivatives of 3-hydroxy-2-[3′, 5′-substituted isoxazole-4′-yl]-4-chromone (**3a-f**, Scheme 1) in good yield. The general reaction sequence involved in the synthesis of 3-hydroxy-2-[3′, 5′-substituted isoxazole-4′-yl]-4-chromone (**3a–f**) is shown in Figure 1. The compounds were characterized by using spectroscopic techniques. Detailed spectroscopic data are provided in Supporting information (Figures S4–S19).

4.2 | Molecular docking studies

Docking was carried out using MAESTRO 9.6 Schrodinger suite. The PDB entries chosen for the studies were 3ERT (Shiau et al., 1998), 2QTU (Richardson et al., 2007), and 2FSZ (Wang et al., 2006). The PDB entry 3ERT chosen is a complex of ERα with 4-hydroxytamoxifen (4HT). The selection of 2QTU entry was based on the structural similarity of the synthesized ligands with benzopyranones. Native ERβ PDB entry is not available; therefore, 2FSZ was selected which is a complex of 4HT with ERβ. Computational tools have been used to elucidate the binding site of compounds. For this, binding affinities of the synthesized compounds with the receptor were compared using ligand interaction map.

The docking of compounds has been studied at ERα, ERβ LBD, and allosteric site. Our studies revealed that the derivatives **3(a-f)** exhibited selectivity for ERα LBD. The significant interacting residues of compounds were compared with the interacting residues of 4HT. Compound **3d** was found to be most potent in the series with -8.71 docking score and has exhibited significant interactions with key residues Arg394 and Glu353. Glu353 and Arg 394 are known to establish H-bonds with a 4-hydroxyphenyl group of 4HT and enhance complex stability [9]; similarly, in our case, we see

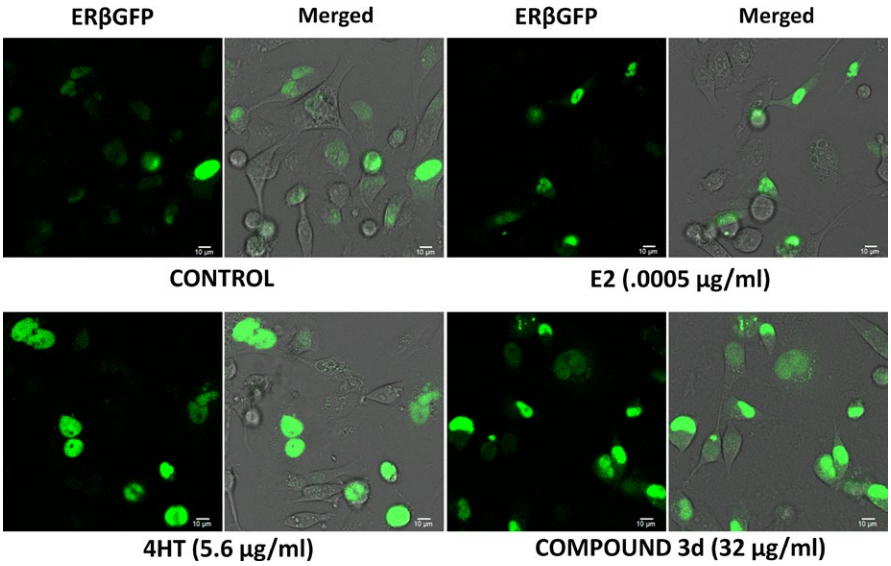

FIGURE 6 ERβ-GFP Reporter Assay: Fluorescence microscopic pictures of GFP-labeled ERβ in breast cancer cells induced with E2, 4HT, and **3d** following 24-hr treatment. Cells on treatment with **3d** emitted enhanced fluorescence as compared to control, E2, and 4HT

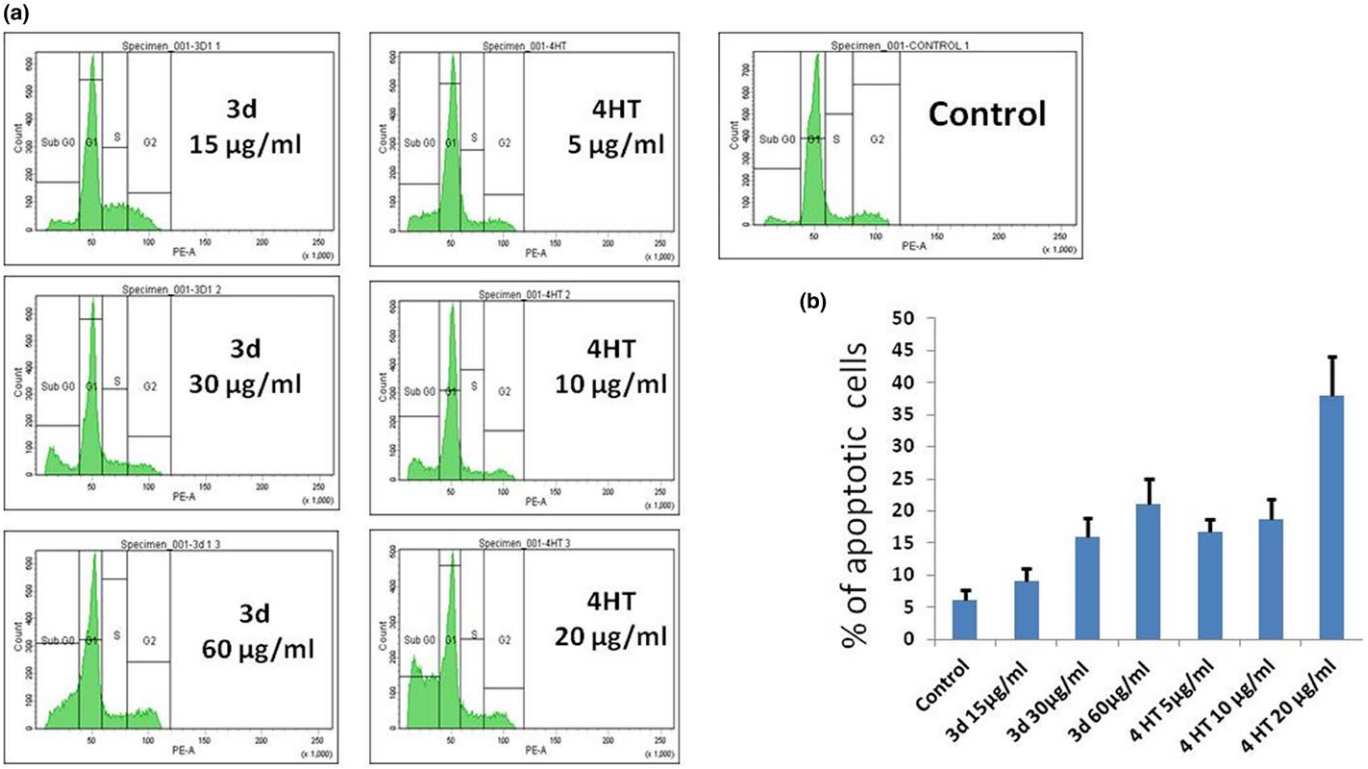

FIGURE 7 (a) Cell cycle analysis: Effect of 4HT and **3d** in MCF-7 cells. Cells were assessed for induction of apoptosis as seen by the increase in the number of cells in sub-G0/G1 phase of cell cycle following 48-hr treatment with HT (5, 10, 20 µg/ml) and **3d** (15, 30, 60 µg/ml) by propidium iodide staining. (b) Data are expressed as Mean±SD of apoptosis expressed as a percentage ($n = 3$). One-way ANOVA where p-value <0.05 is considered significant

interactions of these residues with the phenol hydroxyl group of compound **3d**. The docking score of compounds **3(a–f)** is provided in Table 1.

The ligand interaction map of **3d** exhibiting interactions with ERα and the three-dimensional structure of ERα and ERβ docked with compound **3d** are provided in Figure 2. Comparison of compounds exhibiting interaction with residues in 3ERT is provided in Supporting information (Table S3).

4.3 | Dose-dependent studies

Dose-dependent studies were undertaken on compounds **3(a–f)** in ERα-positive (MCF-7) and ERα-negative (MDA-MB-231 and MRC-5) cell lines as compared to controls using MTT assay. Results indicated preferential cytotoxicity of compound **3(a–f)** in MCF-7 cells. Compound **3d** was found to be most potent with IC_{50} value 31.25 µg/ml. The IC_{50} value of **3(a–f)** on ERα+ (MCF-7) and ERα- (MDA-MB-231) is given in Supporting information (Table S2). The results of the dose-dependent assay are given in Figure 3.

Compound **3d** was found to be a most potent cytotoxic agent against ERα+ cells (MCF-7). Moreover, docking studies with **3d** indicated its selectivity for ERα LBD. Therefore, it was imperative to study **3d** in detail to determine its receptor selective nature. In this regard, other studies were also carried out on **3d** in MCF-7 cells. We have also carried out co-treatment dose-dependent and time-dependent studies of compound **3d** with 4HT. Also, we have determined the antagonistic activity of compound **3d** via modified *E-screen* assay; all results are provided in Supporting information (Figures S1–S3).

4.4 | Gene silencing studies

The above results are indicative that compound **3d** may indeed be exhibiting ER-mediated antagonistic behavior. To confirm the ERα selective nature of **3d,** we have silenced ERα in ERα+ MCF-7 cells using specific siRNA against human ERα. To confirm the silencing, the whole cell extract from silenced and non-silenced cells was prepared. The whole cell extract was separated by electrophoresis, and Western blotting was carried out as described in the Section 2. The specific antibody against ERα was used to detect ERα levels and compared with the housekeeping protein β-actin. As shown in Figure 4A, ERα has been significantly down-regulated in silenced cells compared to control vector transfected MCF-7 cells. The control MCF-7 and silenced cells were exposed to 4HT and compound **3d** for 48 hr followed by analysis of apoptosis by

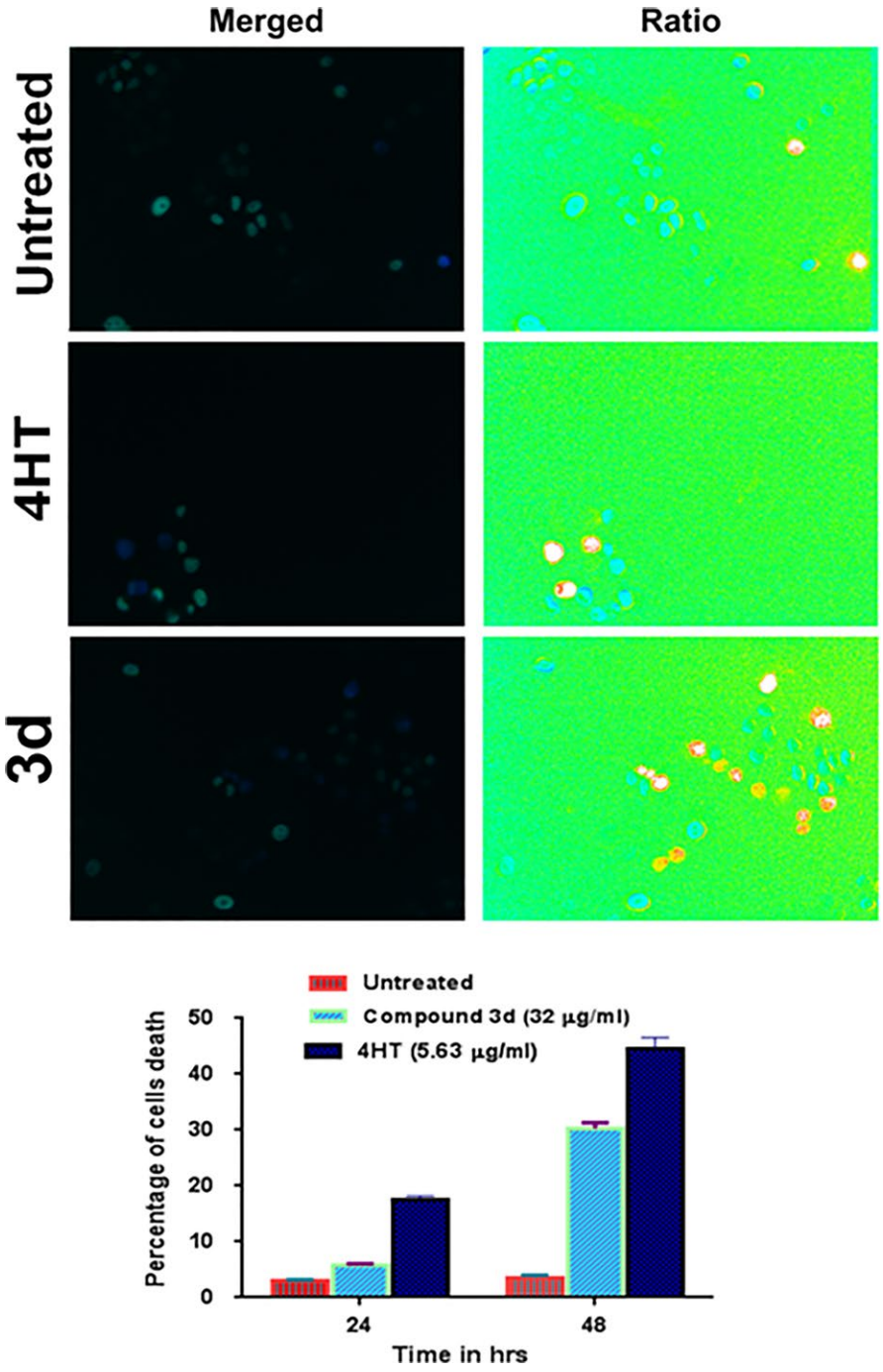

FIGURE 8 Caspase activation analysis: Effect of 4HT and **3d** on triggering caspase-3 activation in MCF-7 SCAT3 NLS cells. Cells were assessed for cell death following 24- and 48-hr treatment with 4HT (5.63 µg/ml) and **3d** (IC_{50} value = 32 µg/ml) by FRET-based assay. (a) Representative images of merged and ratiometric panel after 48 hr of treatment shown. (b) Data are expressed as Mean±SD of cell death expressed as a percentage ($n = 3$). Two-way ANOVA followed by Bonferroni post-test where p-value <0.05 is significant

chromatin condensation as presented in Figure 4b, c. Silencing of ERα reduced cell death induced by 4HT and **3d**.

4.5 | Luciferase reporter gene assay

The above results indicated anti-estrogenic activity of tested compound **3d**. To further validate gene expression in the presence of compound **3d**, ERα-positive MCF-7 cells were transiently transfected with PGL-3-(ERE)-luciferase construct. As depicted in Figure 5, compound **3d** exhibited a decrease in luciferase activity as compared to control at its IC_{50} concentration. These data suggest that **3d**-induced responses are probably mediated through ERα antagonism.

4.6 | ERβ-GFP Reporter Assay

Above results predicted ERα-dependent antagonism of compound **3d**. To further ascertain the ERα selective antagonistic nature of compound **3d**, we carried out ERβ-GFP reporter assay.

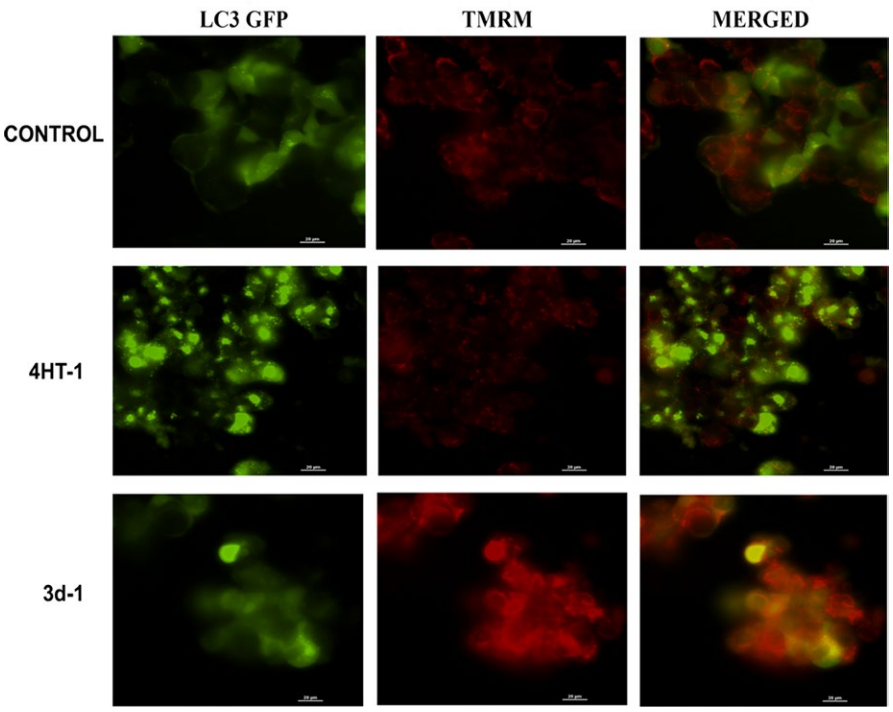

FIGURE 9 LC3 GFP assay: Effect of 4HT-1 (2.81 μg/ml) and **3d**-1(32 μg/ml) on MCF-7 cells expressing LC3 GFP and stained with TMRM (indicates mitochondrial membrane potential). Cells were assessed for autophagy and mitochondrial membrane potential loss following 24-hr treatment with 4HT-1 and **3d**-1

The results indicated a robust signal in the presence of compound **3d** and estradiol (E2), while control cells elicited very little response (fluorescence) as seen in Figure 6. These data confirm that the same compound **3d** has different effects on ERα and ERβ; it is an antagonist to ERα while an agonist to ERβ.

4.7 | Cell cycle analysis by Propidium iodide Staining

The effect of compound **3d** on the cell cycle distribution and sub-G0/G1 phase on MCF-7 cells was measured to determine whether cytotoxicity on ERα is mediated via apoptosis and cell cycle modulation. Treatment with **3d** at 30 and 60 μg/ml induced increase in the number of cells in sub-G0/G1 level as compared to control in MCF-7 cells. This indicates compound **3d** induced cell death via apoptosis similar to 4HT (Figure 7).

4.8 | Cell death pathway

The chromatin condensation results (Figure 4) and cell cycle analysis (Figure 7) indicated that cell death induced by compound **3d** involved apoptosis. Further to confirm pathway of apoptosis, a sensitive live cell caspase activation analysis using ECFP/EYFP-based FRET probe expressing cells was employed. In MCF-7 cells expressing SCAT3 NLS, caspase detection FRET probe was exposed to compound **3d**, as described in Materials and Methods. The result indicated that compound **3d** triggered activation of the caspase-3-mediated cell death pathway with a maximal increase at 48 hr of treatment (Figure 8).

4.9 | LC3 GFP assay for autophagy and mitochondrial membrane potential loss

Treating breast cancer cell line, MCF-7 expressing LC3 GFP failed to show a significant increase in LC3 punctae in **3d**-treated cells compared to untreated cells. However, 4HT at 2.81 μg/ml significantly induced LC3 punctae in treated cells. The percentage of cells with more than 15 punctae per cell scored for 4HT, and **3d** is shown in Figure 9. Interestingly, both **3d** and 4HT induced an almost similar variation in mitochondrial membrane potential (as evident from TMRM staining) in treated cell. The result suggests that **3d** is a dominant cell death inducer with minimum autophagy; however, 4HT simultaneously induced massive survival signaling through the induction of autophagy.

4.10 | Increase in ROS contributed to cell death induced by 3d

MCF-7 cells expressing redox-sensitive GFP was employed to analyze the levels of intracellular ROS induced by **3d**. The redox GFP is a reduction–oxidation sensitive engineered GFP probe that interacts with glutaredoxin and acts as a sensor of cellular redox potential based on the variation in its GFP emission at two distinct excitation wavelengths 405 nm and 488 nm. The cells were exposed to **3d** and 4HT for 24 hr followed by ratio analysis, both by flow cytometry and by microscopy. As shown in Figure 10, treatment of **3d** induced a significant increase in cells with enhanced 405/488 ratios by both flow cytometry and microscopy. 4HT also induced an increase in 405/488 ratio in the majority of

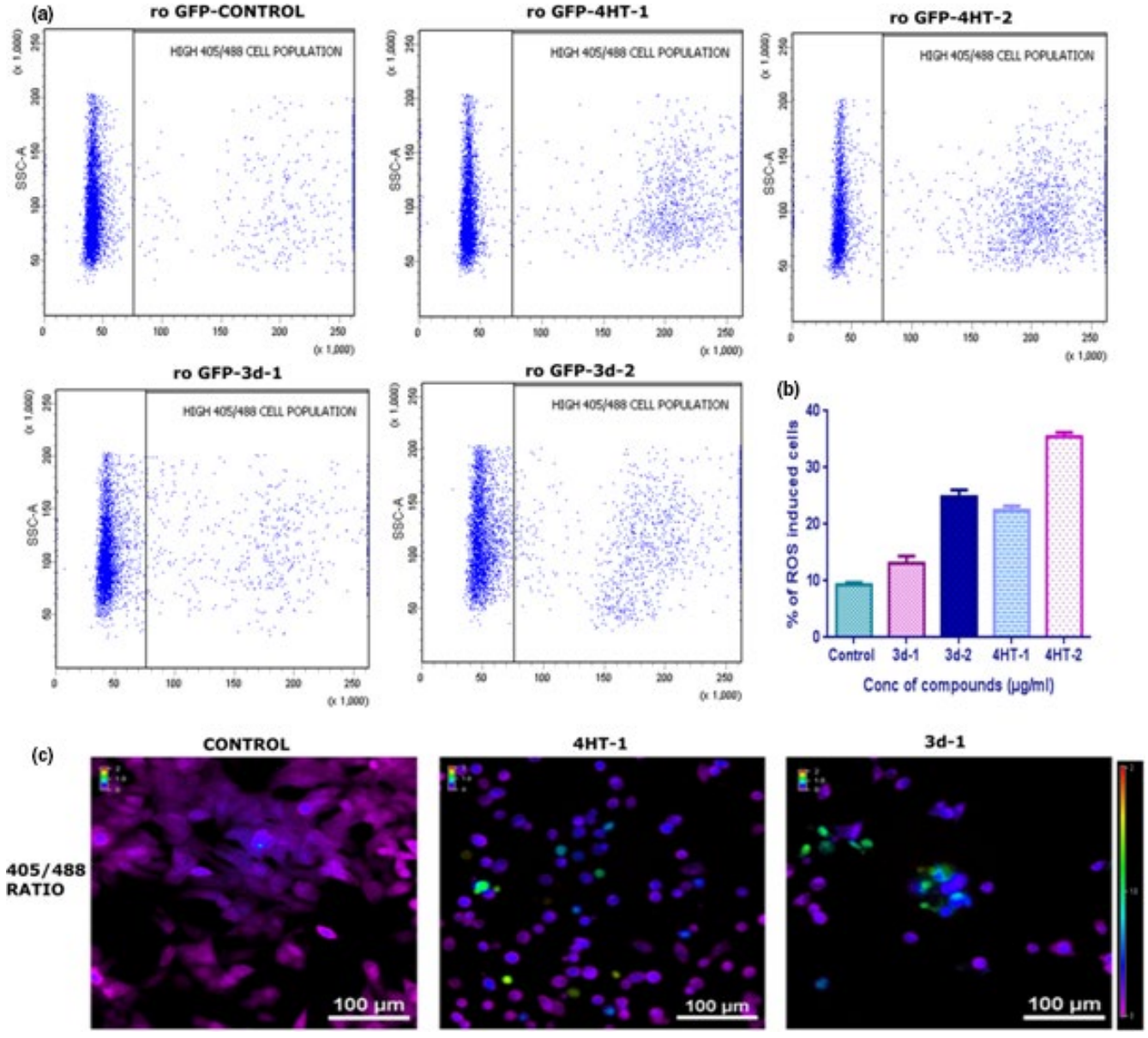

FIGURE 10 (a) ROS analysis: Effect of 4HT and **3d** in MCF-7 cells expressing ratiometric ROS sensing probe, roGFP. Cells were assessed for change in ROS level following 24-hr treatment with HT (HT-1 = 5.63 µg/ml and HT-2 = 9.7 µg/ml) and **3d** (**3d**-1 = 32 µg/ml and **3d**-2 = 62 µg/ml) by ratiometric analysis using FACS. (b) Data are expressed as Mean±SD of cell death expressed as a percentage ($n = 3$). Two-way ANOVA followed by Bonferroni post-test where p-value <0.05 is significant. (c) The effect of 4HT (4HT-1) and **3d** (3d-1) on ROS level was reinforced from the ratiometric images after 24 hr of treatment

cells suggesting ROS as the contributing factor for its cell death.

5 | DISCUSSION

Estrogen receptor signaling plays a critical role in driving ER-positive breast cancer and considered as an important druggable target. Tamoxifen along with second- and third-generation SERMs are currently used in clinical setting for the treatment of ER-positive breast cancer (Maximov et al., 2013). Even though a majority of them proved effective in clinical settings, a subset of breast cancer shows resistance to SERM owing to diverse signaling defects of ERα. In addition, several of the compounds suffer from severe off-target effects such as endocrine resistance, osteoporosis, hot flashes, deep vein thrombosis (DVT), pulmonary embolism, and endometrial cancer (Ellis, Hendrick, Williams, & Komm, 2015; Maximov et al., 2013). Hence, increased attention has been directed toward identifying novel SERM with less off-target effects based on both natural product screening and employing synthetic chemistry. The development of

subtype-selective ligands that specifically target either ERα or ERβ would be a more optimal approach for the treatment of cancer and other diseases such as cardiovascular disease, multiple sclerosis, and Alzheimer's (Nilsson, Koehler, & Gustafsson, 2011). Diverse efforts have been made toward the synthesis of newer ER modulators with increased selectivity toward ERα-positive breast cancer cells and with fewer side-effects. Beside steroid hormones, ER targeting scaffolds include flavones, isoflavones, and coumestans as well as diphenylethylenic derivatives and analogues in the *trans* configuration (Leclercq, Lacroix, Laios, & Laurent, 2006). Grafting of hydrophobic substituents (i.e., phenyl groups) at specific locations in type I estrogens may transform agonists into type II antagonists (Leclercq et al., 2006). Polycyclic compounds containing a phenolic ring and other oxygenated heterocycles located at the opposite end of the molecule where the distance between oxygen is ~11 $Å^3$ have been reported to target ER (Leclercq et al., 2006). Large internal hydrocarbon moiety in these molecules contributes to an optimal orientation of polar functions for selective H-bonding with specific amino acid residues of the ligand-binding pocket (LBD) of ER. Linear, planar molecules are usually ER agonists whereas angular geometry leads to anti-estrogenicity (Leclercq et al., 2006). Reports also suggest molecules that exhibit planar topology and are conformationally rigid usually exhibit ERβ selectivity. Hsieh et al., 2006 reported that ERβ selectivity of oxabicyclic ligands is attributed to the close interaction of ligands with Met-336(ERβ) residue leading to ERβ subtype selectivity. Further, it was also observed that unfavorable interaction with Met421 in ERα resulted in ligands exhibiting ERβ selectivity prominently.

Here, we report the development of isoxazolylchromones as a new class of SERM with strong bioactivity and selectivity toward ERα. The initial docking results indicated that compounds did not exhibit interaction with key residue Met 336 in ERβ; however, all ligands exhibited interaction with Met 421 in ERα. Moreover, several common interactions were found as compared to 4HT in ERα most notably Arg 394. Accordingly, ERα luciferase activity confirmed the antagonistic activity of compound **3d** in relevant breast cancer cell model, MCF-7. The experiments utilizing FRET caspase probe and FACS analysis further confirmed the cytotoxicity and ERα antagonistic potential of the compound in relation to the clinically used SERM, 4HT.

Since we have employed a new approach of chromone scaffold as the building block to synthesize ERα modulators, it has exhibited strong bioactivity and better ERα binding in all the biological assays. A promising feature of **3d** seems to be its ability to induce significant ERβ transactivation. Previous studies have demonstrated that ERα inhibition induces ERβ as a feedback signaling (Saji, Hirose, & Toi, 2005) and ERβ transactivation is known to be advantageous in inhibiting the proliferation potential of hormone-dependent cells involving ERα (Huang, Warner, & Gustafsson, 2015). In addition compared to 4HT, **3d** has failed to induce significant survival signaling in the treated cells involving autophagy. Induction of autophagy is one of the key determinants of hormone resistance (Cook, Shajahan, & Clarke, 2011; Schoenlein, Periyasamy-Thandavan, Samaddar, Jackson, & Barrett, 2009), and several of the clinically approved SERM promote autophagy activity (Samaddar et al., 2008; Viedma-Rodríguez et al., 2014) . Furthermore, we provide evidence that **3d** is the most effective compound that primarily induces ROS-dependent cell death through mitochondrial membrane potential loss and caspase activation. This class of compound is expected to provide an additional class of structurally different new SERM for further development and testing in preclinical models in the best interest of the development of new SERM.

In summary, we report synthesis and validation of a new class of isoxazolylchromones **3(a–f)** as a novel ERα selective agent with promising bioactivity based on a different structural design, as evident from bioactivity profiling, selectivity studies, and comparative in vitro cytotoxicity results. The results confirm its utility as an ER isoform selective agent with the potential to be developed as possible SERMs. Further studies are ongoing to substantiate their off-target effects and clinical potential in patient-derived samples.

ACKNOWLEDGMENTS

SK thanks SERB-NPDF (PDF/2016/004001) for financial assistance. All authors gratefully acknowledge Prof. M. Radhakrishna Pillai, Director, Rajiv Gandhi Centre for Biotechnology, Trivandrum, for his support. Authors also gratefully acknowledge the guidance of Dr.Damoder Gupta, INMAS, for cytotoxicity studies. Authors acknowledge Amity Institute of Biotechnology, Amity University, for infrastructure and other facilities. Support to the Cancer Research Program 1, Rajiv Gandhi Centre for Biotechnology, Trivandrum, by Department of Biotechnology (BT/PR8087/MED/32/292/2013), Government of India, is also gratefully acknowledged. SK also acknowledges Prakash R. Pillai, Technical Assistance, Rajiv Gandhi Centre for Biotechnology, Trivandrum, for his timely assistance.

CONFLICT OF INTEREST

The author(s) declare no competing interests.

ORCID

Thankayyan Retnabai Santhoshkumar https://orcid.org/0000-0003-3386-7105

REFERENCES

Banks, J. L., Beard, H. S., Cao, Y., Cho, A. E., Damm, W., Farid, R., … Levy, R. M. (2005). Integrated modeling program, applied chemical theory (IMPACT). *Journal of Computational Chemistry*, *26*, 1752–1780. https://doi.org/10.1002/jcc.20292

Beato, M., Herrlich, P., & Schütz, G. (1995). Steroid hormone receptors: Many actors in search of a plot. *Cell*, *83*, 851–857. https://doi.org/10.1016/0092-8674(95)90201-5

Chang, B. Y., Kim, S. A., Malla, B., & Kim, S. Y. (2011). The effect of selective estrogen receptor modulators (SERMs) on the tamoxifen resistant breast cancer cells. *Toxicology Research*, *27*, 85–93. https://doi.org/10.5487/TR.2011.27.2.085

Cook, K. L., Shajahan, A. N., & Clarke, R. (2011). Autophagy and endocrine resistance in breast cancer. *Expert Review of Anticancer Therapy*, *11*, 1283–1294. https://doi.org/10.1586/era.11.111

Das, B., Mahender, G., Holla, H., & Banerjee, J. (2005). An easy access to 3a,4-dihydro-3H-chromeno[4,3-c]isoxazoles and functionalized isoxazolines. *ARKIVOC*, *3*, 27–35.

Ellis, A. J., Hendrick, V. M., Williams, R., & Komm, B. S. (2015). Selective estrogen receptor modulators in clinical practice: A safety overview. *Expert Opinion in Drug Safety*, *14*, 921–934. https://doi.org/10.1517/14740338.2015.1014799

Farhat, M. Y., Lavigne, M. C., & Ramwell, P. W. (1996). The vascular protective effects of estrogen. *The FASEB Journal*, *10*, 615–624.

Heldring, N., Pike, A., Andersson, S., Mathews, J., Cheng, G., Hartman, J., … Gustafsson, J. A. (2007). Estrogen receptors: How do they signal and what are their targets. *Physiological Reviews*, *87*, 905–931. https://doi.org/10.1152/physrev.00026.2006

Henderson, B. E., & Feigelson, H. S. (2000). Hormonal carcinogenesis. *Carcinogenesis*, *21*, 427–433. https://doi.org/10.1093/carcin/22.3.529

Hongyi, Q., Zhuyun, J., Chengqiang, W., Yang, Y., Li, L., Hui, H., & Zanyang, Y. (2017). Sensitization of tamoxifen-resistant breast cancer cells by Z-ligustilide through inhibiting autophagy and accumulating DNA damages. *Oncotarget*, *8*, 29300–29317. https://doi.org/10.18632/oncotarget.16832

Hsieh, R. W., Rajan, S. S., Sharma, S. K., Guo, Y., DeSombre, E. R., Mrksich, M., & Greene, G. L. (2006). Identification of ligands with bicyclic scaffolds provides insights into mechanisms of estrogen receptor subtype selectivity. *The Journal of Biological Chemistry*, *281*, 17909–17919. https://doi.org/10.1074/jbc.M513684200

Huang, B., Warner, M., & Gustafsson, J. A. (2015). Estrogen receptors in breast carcinogenesis and endocrine therapy. *Molecular and Cellular Endocrinology*, *418*, 240–444. https://doi.org/10.1016/j.mce.2014.11.015

Joseph, J., Seervi, M., Sobhan, P. K., & Santhoshkumar, T. R. (2011). High throughput ratio imaging to profile caspase activity: Potential application in multiparameter high content apoptosis analysis and drug screening. *PLoS ONE*, *6*, 1–17. https://doi.org/10.1371/journal.pone.0020114

Kuiper, G. G., Carlsson, B., Grandien, K., Enmark, E., Häggblad, J., Nilsson, S., & Gustafsson, J. A. (1997). Comparison of the ligand binding specificity and transcript tissue distribution of estrogen receptors alpha and beta. *Endocrinology*, *138*, 863–70. https://doi.org/10.1210/endo.138.3.4979

Laïos, I., Cleeren, A., Leclercq, G., Nonclercq, D., Laurent, G., Schlenk, M., … Gust, R. (2007). Effects of (R, S)/(S, R)-4,5-bis(2-chloro-4-hydroxyphenyl)-2-imidazolines and (R, S)/(S, R)-2,3-bis(2-chloro-4-hydroxyphenyl) piperazines on estrogen receptor alpha level and transcriptional activity in MCF-7 cells. *Biochemical Pharmacology*, *74*, 1029–38. https://doi.org/10.1016/j.bcp.2007.06.045

Leclercq, G., Lacroix, M., Laios, I., & Laurent, G. (2006). Estrogen receptor alpha: Impact of ligands on intracellular shuttling and turnover rate in breast cancer cells. *Current Cancer Drug Targets*, *6*, 39–64. https://doi.org/10.2174/156800906775471716

Masood, S. (1992). Estrogen and progesterone receptors in cytology: A comprehensive review. *Diagnostic Cytopathology*, *8*, 475–491. https://doi.org/10.1002/dc.2840080508

Maximov, P. Y., Lee, T. M., & Jordan, V. C. (2013). The discovery and development of selective estrogen receptor modulators (SERMs) for clinical practice. *Current Clinical Pharmacology*, *8*, 135–155. https://doi.org/10.2174/1574884711308020006

Middleton, E. Jr., Kandaswami, C., & Theoharides, T. C. (2000). The effects of plant flavonoids on mammalian cells: Implications for inflammation, heart disease, and cancer. *Pharmacological Reviews*, *52*, 673–751.

Minutolo, F., Macchia, M., Katzenellenbogen, B. S., & Katzenellenbogen, J. A. (2011). Estrogen receptor β ligands: Recent advances and biomedical applications. *Medicinal Research Reviews*, *31*, 364–442. https://doi.org/10.1002/med.20186

Momoi, K., Sugita, Y., Ishihara, M., Satoh, K., Kikuchi, H., Hashimoto, K., … Sakagami, H. (2005). Cytotoxic activity of styrylchromones against human tumor cell lines. *In Vivo*, *19*, 157–163.

Nilsson, S., Koehler, K. F., & Gustafsson, J. A. (2011). Development of subtype-selective oestrogen receptor-based therapeutics. *Nature Reviews Drug Discovery*, *10*, 778–792. https://doi.org/10.1038/nrd3551

Nilsson, S., Makela, S., Treuter, E., Tujague, M., Thomsen, J., Andersson, G., … Gustafsson, J. A. (2001). Mechanism of estrogen action. *Physiological Reviews*, *81*, 1535–1565. https://doi.org/10.1152/physrev.2001.81.4.1535

Ottow, E., & Weinmann, H. (2008). *Nuclear receptors as drug targets: A historical perspective of modern drug discovery*. New York, NY: Wiley-VCH Verlag GmbH & Co. KGaA, Wiley Publications.

Paterni, I., Granchi, C., Katzenellenbogen, J. A., & Minutolo, F. (2014). Estrogen receptors alpha (ERα) and beta (ERβ): Subtype-selective ligands and clinical potential. *Steroids*, *90*, 13–29. https://doi.org/10.1016/j.steroids.2014.06.012

Peng, J., Sengupta, S., & Jordan, V. C. (2009). Potential of selective estrogen receptor modulators as treatments and preventives of breast cancer. *Anti-cancer Agents in Medicinal Chemistry*, *9*, 481–99.

Pick, A., Müller, H., Mayer, R., Haenisch, B., Pajeva, I. K., Weigt, M., … Wiese, M. (2011). Structure-activity relationships of flavonoids as inhibitors of breast cancer resistance protein (BCRP). *Bioorganic & Medicinal Chemistry*, *19*, 2090–2102. https://doi.org/10.1016/j.bmc.2010.12.043

Richardson, T. I., Norman, B. H., Lugar, C. W., Jones, S. A., Wang, Y., Durbin, J. D., … Dodge, J. A. (2007). Benzopyrans as selective estrogen receptor beta agonists (SERBAs). Part 2: Structure-activity relationship studies on the benzopyran scaffold. *Bioorganic & Medicinal Chemistry Letters*, *17*, 3570–3574. https://doi.org/10.1016/j.bmcl.2007.04.051

Saji, S., Hirose, M., & Toi, M. (2005). Clinical significance of estrogen receptor beta in breast cancer. *Cancer Chemotherapy and Pharmacology*, *56*, 21–26. https://doi.org/10.1007/s00280-005-0107-3

Samaddar, J. S., Gaddy, V. T., Duplantier, J., Thandavan, S. P., Shah, M., Smith, M. J., … Schoenlein, P. V. (2008). A role for macroautophagy

in protection against 4-hydroxytamoxifen-induced cell death and the development of antiestrogen resistance. *Molecular Cancer Therapeutics*, *7*, 2977–2987. https://doi.org/10.1158/1535-7163.MCT-08-0447

Schoenlein, P. V., Periyasamy-Thandavan, S., Samaddar, J. S., Jackson, W. H., & Barrett, J. T. (2009). Autophagy facilitates the progression of ER alpha-positive breast cancer cells to antiestrogen resistance. *Autophagy*, *5*, 400–403. https://doi.org/10.4161/auto.5.3.7784

Shiau, A. K., Barstad, D., Loria, P. M., Cheng, L., Kushner, P. J., Agard, D. A., & Greene, G. L. (1998). The structural basis of estrogen receptor/coactivator recognition and the antagonism of this interaction by tamoxifen. *Cell*, *95*, 927–37. https://doi.org/10.1016/S0092-8674(00)81717-1

Sommer, S., & Fuqua, S. A. (2001). Estrogen receptor and breast cancer. *Seminars in Cancer Biology*, *11*, 339–352. https://doi.org/10.1006/scbi.2001.0389

Turner, R. T., Riggs, B. L., & Spelsberg, T. C. (1994). Skeletal effects of estrogen. *Endocrine Reviews*, *15*, 275–300. https://doi.org/10.1210/edrv-15-3-275

Viedma-Rodríguez, R., Baiza-Gutman, L., Salamanca-Gómez, F., Diaz-Zaragoza, M., Martínez-Hernández, G., Ruiz Esparza-Garrido, R., … Arenas-Aranda, D. (2014). Mechanisms associated with resistance to tamoxifen in estrogen receptor-positive breast cancer. *Oncology Reports*, *32*, 3–15. https://doi.org/10.3892/or.2014.3190

Wang, Y., Chirgadze, N. Y., Briggs, S. L., Khan, S., Jensen, E. V., & Burris, T. P. (2006). A second binding site for hydroxytamoxifen within the coactivator-binding groove of estrogen receptor beta. *Proceedings of the National Academy of Sciences USA*, *103*, 9908–9911. https://doi.org/10.1073/pnas.0510596103

SUPPORTING INFORMATION

Additional supporting information may be found online in the Supporting Information section at the end of the article.

How to cite this article: Kaushik S, Sanawar R, Lekshmi A, et al. ER alpha selective chromone, isoxazolylchromones, induces ROS-mediated cell death without autophagy. *Chem Biol Drug Des*. 2019;00:1–16. https://doi.org/10.1111/cbdd.13510